AD NUMBER

AD845053

LIMITATION CHANGES

TO:

Approved for public release; distribution is unlimited.

FROM:

**Distribution authorized to U.S. Gov't. agencies and their contractors;
Administrative/Operational Use; DEC 1968. Other requests shall be referred to Arnold Engineering Development Center, Arnold AFB, TN.**

AUTHORITY

AEDC ltr, 26 Apr 1973

AEDC-TR-68-277

DYNAMIC STABILITY RESULTS FOR SHARP AND BLUNTED 10-DEG CONES AT HYPERSONIC SPEEDS

L. K. Ward, Jr. and B. L. Uselton

ARO, Inc.

December 1968

VON KÁRMÁN GAS DYNAMICS FACILITY
ARNOLD ENGINEERING DEVELOPMENT CENTER
AIR FORCE SYSTEMS COMMAND
ARNOLD AIR FORCE STATION, TENNESSEE

NOTICES

When U. S. Government drawings specifications, or other data are used for any purpose other than a definitely related Government procurement operation, the Government thereby incurs no responsibility nor any obligation whatsoever, and the fact that the Government may have formulated, furnished, or in any way supplied the said drawings, specifications, or other data, is not to be regarded by implication or otherwise, or in any manner licensing the holder or any other person or corporation, or conveying any rights or permission to manufacture, use, or sell any patented invention that may in any way be related thereto.

Qualified users may obtain copies of this report from the Defense Documentation Center.

References to named commercial products in this report are not to be considered in any sense as an endorsement of the product by the United States Air Force or the Government.

ARNOLD ENGINEERING DEVELOPMENT CENTER
AIR FORCE SYSTEMS COMMAND
UNITED STATES AIR FORCE
ARNOLD AIR FORCE STATION, TENNESSEE

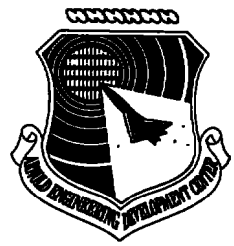

TRANSMITTAL NOTE

1. The attached report is forwarded for your information and retention.

2. Inquiries relative to any feature of this report should be addressed to this Headquarters, ATTN: AETS.

ROY R. CROY, JR., Colonel, USAF
Director of Test

DYNAMIC STABILITY RESULTS FOR SHARP AND BLUNTED 10-DEG CONES AT HYPERSONIC SPEEDS

L. K. Ward, Jr. and B. L. Uselton
ARO, Inc.

FOREWORD

The work reported herin was sponsored by the Arnold Engineering Development Center (AEDC), Air Force Systems Command (AFSC), Arnold Air Force Station, Tennessee, under Program Element 65401F/G226.

Results of the research presented were obtained by ARO, Inc., (a subsidiary of Sverdrup & Parcel and Associates, Inc.), contract operator of AEDC under Contract F40600-69-C-0001. The research was done from June 30, 1967, to June 30, 1968, under ARO Project No. VT0878, and the manuscript was submitted for publication on November 13, 1968.

This technical report has been reviewed and is approved.

Eugene C. Fletcher
Lt Colonel, USAF
AF Representative, VKF
Directorate of Test

Roy R. Croy, Jr.
Colonel, USAF
Director of Test

ABSTRACT

Tests were conducted in Tunnel C of the von Kármán Gas Dynamics Facility to obtain dynamic stability data for sharp and blunted 10-deg half-angle cones. With both a free-oscillation gas bearing pivot balance system and a forced-oscillation cross-flexure pivot balance system, data were obtained at a nominal Mach number of 10 at free-stream Reynolds numbers, based on model length, ranging from 1.80×10^6 to 3.19×10^6. The effects of boundary-layer transition, amplitude of oscillation, nose bluntness, and model center-of-gravity location on the dynamic and static stability derivatives are presented. Comparison of data from the free- and forced-oscillation test techniques and the effect of frequency of oscillation on the damping-in-pitch derivatives are also presented. The derivatives are compared with steady and unsteady flow field theories.

CONTENTS

APPENDIXES

NOMENCLATURE

A	Reference area (model base area), ft^2
C_N	Normal-force coefficient, normal force/q_∞ A
C_{N_α}	$\partial C_N/\partial\alpha$, 1/rad
C_m	Pitching-moment coefficient, pitching moment/q_∞ Ad
C_{m_q}	$\partial C_m/\partial(qd/2V_\infty)$, 1/rad
C_{m_α}	$\partial C_m/\partial\alpha$, 1/rad
$C_{m_{\dot\alpha}}$	$\partial C_m/\partial(\dot\alpha d/2V_\infty)$, 1/rad

} Effective values

d	Reference length (model base diameter), ft
L	Virtual model length (see Fig. 5), ft
ℓ	Actual model length (see Fig. 5), ft
M_∞	Free-stream Mach number
q	Pitching velocity, rad/sec
q_∞	Free-stream dynamic pressure, lb/ft^2
Re_L	Free-stream Reynolds number based on virtual model length
Re_ℓ	Free-stream Reynolds number based on model length
Re/ℓ	Free-stream unit Reynolds number, 1/ft
r_b	Model base radius, in.
r_n	Model nose radius, in.
V_∞	Free-stream velocity, ft/sec
X_{cg}	Distance from virtual model nose to pivot axis (see Fig. 5), ft
x_{cg}	Distance from model nose to pivot axis (see Fig. 5), ft
α	Angle of attack, rad
$\dot\alpha$	Time rate of change of angle of attack, rad/sec
θ	Oscillation amplitude, deg

θ_c Cone half-angle, deg

ω Angular frequency, rad/sec

$\omega d/2V_\infty$ Reduced frequency parameter, rad

SUBSCRIPT

o Moment reference at the nose

SECTION I
INTRODUCTION

The purpose of this report is to present recent dynamic stability data that were obtained on sharp and blunted 10-deg half-angle cones in the 50-in. VKF tunnel (Gas Dynamic Wind Tunnel, Hypersonic (C)) at a nominal Mach number of 10.

The measurements were made at a free-stream Reynolds number that was sufficiently low to provide a laminar boundary layer on the model surface when the model was oscillating ±2 deg. For completeness of the report, the effects of Reynolds number, or rather the effects of boundary-layer transition, on the static and dynamic derivatives will be reviewed. In addition, the effects of oscillation amplitude and center-of-gravity location on the static and dynamic stability derivatives will be shown along with the effects of frequency of oscillation on the pitch derivatives at Mach 10. The data will be compared with predictions of steady (static stability only) and unsteady flow field theories.

SECTION II
APPARATUS

2.1 WIND TUNNEL

Tunnel C is a continuous, closed-circuit, variable density wind tunnel with an axisymmetric contoured nozzle and a 50-in.-diam test section. The tunnel can be operated at a nominal Mach number of 10 or 12 at stagnation conditions from 200 to 1850 psia at 1900°R and from 600 to 2000 psia at 2350°R, respectively. The model may be injected into the tunnel for a test run and then retracted for model cooling or model changes without interrupting the tunnel flow. A description of the tunnel may be found in Ref. 1. A summary of the test conditions is given in Table I (Appendix II).

2.2 BALANCES

2.2.1 Free-Oscillation Balance

The one-degree-of-freedom dynamic balance used in the present tests is a large amplitude (±15-deg) system incorporating a cylindrical gas bearing as the pivot. The balance has an angular transducer which provides an analog signal proportional to model amplitude, yet requires no physical contact between the moving and stationary parts of the bearing. A more complete description of the system may be found in Ref. 2.

2.2.2 Forced-Oscillation Balance

The small amplitude (±3-deg) forced-oscillation balance system used in the present tests is a one-degree-of-freedom oscillatory system incorporating a cross-flexure pivot and is forced to oscillate by an electromagnetic shaker motor. Additional information concerning the balance may be found in Ref. 2.

2.3 MODEL

The model used in the present tests was a 10-deg half-angle cone ($d \approx 10$ in.) and had a series of removable noses to provide nominal bluntness ratios (r_n/r_b) of 0, 0.15, and 0.3. The model was balanced so that the model balance center of gravity was located at the balance pivot axis.

SECTION III
DATA REDUCTION

3.1 FREE-OSCILLATION TESTS

Neither the static nor the dynamic derivatives for the blunted cones were constant with oscillation amplitude. The differential equation describing the motion is, therefore, nonlinear. The log decrement technique (linear theory) may still be used in cases when the aerodynamic stiffness (C_{m_α}) is linear by applying the linear theory over small time increments where the motion is nearly exponentially damped. When the aerodynamic stiffness varies with oscillation amplitude, errors in the damping factor are introduced by using the linear theory as shown by Nicolaides in Ref. 3. The complete nonlinear data reduction techniques used in these tests are presented in detail in Ref. 4.

3.2 FORCED-OSCILLATION TESTS

The forced-oscillation data were obtained at the natural undamped frequency of the model-balance system. The models were oscillated in a vacuum chamber at pressures ranging from 0.5 psia to atmospheric pressure in order to determine the damping resulting from ambient pressure. The complete data reduction procedures may be found in Ref. 4.

SECTION IV
RESULTS AND DISCUSSION

4.1 EFFECTS OF BOUNDARY-LAYER TRANSITION

During the course of an experimental study to determine the effects of support interference on the dynamic stability of a sharp 10-deg cone at supersonic speeds, Uselton (Ref. 5) found that there existed a consistent rise in the damping derivatives ($C_{m_q} + C_{m_{\dot{\alpha}}}$) and fall in the static derivative (C_{m_α}) as shown in the sketch below. The maximum and minimum values of $C_{m_q} + C_{m_{\dot{\alpha}}}$ and C_{m_α}, respectively, were found to occur when boundary-layer transition, (the beginning of fully developed turbulent flow) as detected by schlieren photographs and base pressure measurements, was near the model base. Reynolds number had no effect on the static or dynamic derivatives if the model boundary layer remained laminar or near fully turbulent throughout the model oscillation amplitude range. These same trends were observed by Ward at hypersonic speeds as reported in Ref. 6. Typical data from the above sources are shown in Fig. 1 (Appendix I).

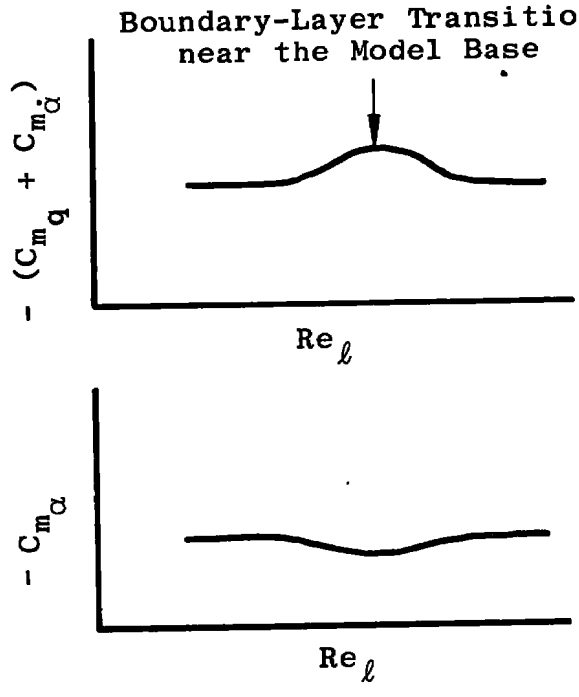

Jaffee and Prislin conducted wind tunnel tests at the Jet Propulsion Laboratory (JPL) using the wind tunnel free-flight technique in order to investigate the effect of boundary-layer transition on the dynamic stability of sharp, 10-deg half-angle cones (Ref. 7). A conclusion reached during the course of that work was that the nature of the boundary layer and the position of transition did not affect the dynamic stability of 10-deg half-angle cones. Later work, however, at JPL by Prislin (Ref. 8) using 10-deg half-angle cones led him to conclude that Reynolds number had a significant influence on the dynamic stability of sharp cones.

In the earlier JPL work mentioned above (Ref. 7), a series of boundary-layer trips was used to promote transition and to provide

several "effective" Reynolds numbers for one free-stream tunnel condition. Studies were made only at zero angle of attack when the trip sizes were selected, and estimates were made where transition would be moved for the maximum trip diameter used. It is well documented (for example, see Refs. 6, 9, and 10) that as a cone is yawed, transition will move forward on the leeside and slightly rearward on the wind side. McCauley et al. (Ref. 10) have shown, however, that when trips are used the reverse may be true. This is readily apparent when one considers the physical situation at the trip location on a yawed cone. The boundary layer on the windward side has thinned making the trip more effective, whereas the boundary layer on the leeside has become thicker making the trip less effective. It is certainly probable that boundary-layer trips could subdue or even reverse the established trends noted in the sketch and explained by Ericsson in Ref. 11 as being caused by viscous time-lag effects.

Now that the effects of boundary-layer transition on the static and dynamic stability of cones have been established, it should become clear that one should not consider this a Reynolds number effect when attempting to compare data from one tunnel to another. Rather, the data should be compared on the basis of the transition Reynolds numbers for each wind tunnel. Pate and Schueler provide in Ref. 12 conclusive proof that transition Reynolds number is a function of tunnel size. It should also be apparent that when wind tunnel data are compared with theory, one should compare data obtained either before or after the rise in the dynamic stability as depicted in the sketch.

4.2 EFFECTS OF NOSE BLUNTNESS

Typical dynamic and static stability data obtained on a 10-deg half-angle cone during the present tests at $M_\infty \approx 10$ with bluntness ratios (r_n/r_b) of 0.001, 0.151, and 0.300 are shown in Fig. 2 as a function of oscillation amplitude. These data are from models tested with the center of gravity at a point 60 percent aft of the virtual length of the cone ($X_{cg}/L = 0.60$). The damping derivatives ($C_{m_q} + C_{m_{\dot\alpha}}$) and static stability derivatives (C_{m_α}) for the sharp cone were constant over the amplitude range tested. For the blunted cones, the static stability derivative was not constant with oscillation amplitude (θ) but decreased with amplitude for $r_n/r_b = 0.151$ and increased with amplitude for $r_n/r_b = 0.300$. The damping for both blunted cones increased with amplitude. The unsteady flow field theory (Refs. 13 and 14) agrees well with all derivatives as θ approaches zero, although the theory predicts somewhat lower values of damping ($C_{m_q} + C_{m_{\dot\alpha}}$) and somewhat higher values of C_{m_α} for the blunted cones.

Although not shown, similar trends with amplitude were found for the static and dynamic derivatives (C_{m_α} and $C_{m_q} + C_{m_{\dot\alpha}}$) at $M_\infty = 10$

with the pivot axis at 65 percent of the cone virtual length (X_{cg}/L = 0.65). The levels of the derivatives obtained at $\theta = \pm 2$ deg are shown in Fig. 3 as a function of nose bluntness ratio (r_n/r_b) and are compared with the unsteady flow field theory (Ref. 14). Again, the agreement with theory is best for the sharp cone data. It is interesting to note the variation with nose bluntness that the theory predicts for both $C_{m_q} + C_{m_{\dot{\alpha}}}$ and C_{m_α}. Additional experimental data are needed at bluntness ratios between $r_n/r_b = 0$ and 0.15 to confirm the trends predicted by the theory.

Clay conducted experiments at $M_\infty = 14.2$ at the Aerospace Research Laboratory (Ref. 15) to determine the effects of nose bluntness on $C_{m_q} + C_{m_{\dot{\alpha}}}$ and C_{m_α} of a 10-deg half-angle cone. These data are compared in Fig. 4 with flow field theory (Ref. 14). The model moment reference point (model pivot axis) was held constant with respect to the cone virtual length at $X_{cg}/L = 0.608$. The measured damping derivatives ($C_{m_q} + C_{m_{\dot{\alpha}}}$) agree with the theory at $r_n/r_b = 0$ and 0.15 and are higher than the theory at $r_n/r_b = 0.30$, as was the case with the present $M_\infty = 10$ data in Fig. 3. At $r_n/r_b < 0.15$, the trend predicted by the theory was not confirmed by these data. The C_{m_α} data were in better agreement with the trend predicted by the theory.

It is interesting to observe that the original work done by Brong (Ref. 13) on the unsteady flow field solutions for a sharp cone yeilded C_{N_α} values which agreed precisely with the Stone-Kopal results (referred to herein as Conical Flow Theory) for the steady-state solution. The extension of Brong's work to include blunted cones as reported by Rie et al. in Ref. 14 provides a C_{N_α} value that does not approach the Conical Flow Theory as r_n/r_b approaches zero. The theoretical values, C_{N_α} and C_{m_α}, from Ref. 14 are shown in Fig. 5 as a function of r_n/r_b for a 10-deg cone at $M_\infty = 10$. One may see that C_{N_α} does not approach the level provided by Conical Flow Theory. Note the Conical Flow Theory for C_{m_α} (Fig. 5). This curve was obtained by ignoring the physical nose bluntness of the cone and determining the distance to the center of gravity from the virtual nose of the cone (X_{cg}) and using the virtual length of the cone (L) to obtain X_{cg}/L. Values of C_{m_α} may then be obtained by using the following well-known equations for sharp cones:

$$C_{m_\alpha} = C_{m_{\alpha o}} + \left(\frac{X_{cg}}{L} C_{N_\alpha}\right) \frac{L}{d}$$

where

$$C_{m_{\alpha o}} = -\frac{2}{3} \sec^2 \theta_c \, C_{N_\alpha} \frac{L}{d}$$

and

$$C_{m_\alpha} = \left(\frac{X_{cg}}{L} - \frac{2}{3} \sec^2 \theta_c\right) C_{N_\alpha} \frac{L}{d}$$

It would seem that this approximation for C_{m_α} may be a more valid estimate than the unsteady flow field theory of Ref. 14 if one limits its use to very small values of r_n/r_b. The limit for this case (θ_c = 10 deg, M_∞ = 10) would appear from Fig. 5 to be $r_n/r_b \approx 0.07$. In addition, one must use caution when comparing experimental results of near sharp cones with the theory for sharp cones and should ensure that the proper reference lengths are used.

The unsteady flow field theory of Ref. 14 has been plotted in Fig. 6 to show the effects of nose bluntness on $C_{m_q} + C_{m_{\dot\alpha}}$ and C_{m_α} for a 10-deg half-angle cone at M_∞ = 10 for x_{cg}/ℓ values ranging from 0.52 to 0.68.

4.3 EFFECTS OF CENTER-OF-GRAVITY LOCATION

The variations of the damping derivatives ($C_{m_q} + C_{m_{\dot\alpha}}$) with center-of-gravity location (x_{cg}/ℓ) for sharp and blunted 10-deg half-angle cones at M_∞ = 10 are shown in Fig. 7. The data were obtained at oscillation amplitudes (θ) of about ±2 deg using the forced- and the free-oscillation techniques. The experimental data for r_n/r_b = 0.001 appear to be scattered about the level of the unsteady flow field theory (Ref. 13). The data for r_n/r_b = 0.151 are slightly above the theory (Ref. 14), whereas the level of the r_n/r_b = 0.300 data is twice the level predicted by the theory.

The effect of center-of-gravity location (x_{cg}/ℓ) on cone static stability derivatives is shown in Fig. 8 as obtained by using both the free- and forced-oscillation techniques. The sharp cone data agree almost precisely with the unsteady flow field theory (Ref. 13). The r_n/r_b = 0.300 data agree well with the theory (Ref. 14), but the same theory overpredicts the level of C_{m_α} measured for r_n/r_b = 0.151.

4.4 EFFECTS OF REDUCED FREQUENCY

Figure 9 shows the effects of reduced frequency ($\omega d/2V_\infty$) on the damping derivatives ($C_{m_q} + C_{m_{\dot\alpha}}$) for 10-deg cones with bluntness ratios (r_n/r_b) of 0.001, 0.151, and 0.300. The data were obtained at M_∞ = 10 and at free-stream Reynolds numbers (Re_ℓ) ranging from 1.80×10^6 to 3.19×10^6 using the free- and forced-oscillation techniques. The data show that the damping derivatives increased with $\omega d/2V_\infty$ at some exponential rate. No conclusion on the effects of $\omega d/2V_\infty$ on the damping derivatives will be drawn at this time. It does appear that additional experiments are needed to confirm these trends and to extend the range of $\omega d/2V_\infty$.

REFERENCES

1. Test Facilities Handbook (7th Edition. "von Kármán Gas Dynamics Facility, Vol. 4." Arnold Engineering Development Center, July 1968.

2. Hodapp, A. E., Jr., Uselton, B. L., and Burt, G. E. "Dynamic Stability Characteristics of a 10-deg Cone at Mach Number 10." AEDC-TDR-64-98 (AD440188), May 1964.

3. Nicolaides, J. D. "Missile Flight and Astrodynamics." U.S. Bureau of Weapons, Department of the Navy, TN-100A, 1959-61.

4. Schueler, C. J., Ward, L. K., and Hodapp, A. E. "Techniques for Measurement of Dynamic Stability Derivatives in Ground Test Facilities." AGARDograph 121, October 1967.

5. Uselton, B. L. "Investigation of Sting Support Interference Effects on the Dynamic and Static Stability Characteristics of a 10-deg Cone at Mach Numbers 2.5, 3, and 4." AEDC-TDR-64-226 (AD450660), November 1964.

6. Ward, L. K. "Influence of Boundary Layer Transition on Dynamic Stability at Hypersonic Speeds." Transactions of the Second Technical Workshop on Dynamic Stability Testing, Arnold Engineering Development Center, Vol. II (AD472298), April 20-22, 1965.

7. Jaffe, P. and Prislin, R. H. "Effect of Boundary Layer Transition on Dynamic Stability." Journal of Spacecraft Rockets, Vol. 3, January 1966, pp. 46-52.

8. Prislin, Robert H. "High-Amplitude Dynamic Stability Characteristics of Blunt 10-Degree Cones." JPL-TR-32-1012, October 1966.

9. Jack, John R. and Moskowitz, Barry. "Experimental Investigation of Temperature Recovery Factors on a 10-deg Cone at Angles of Attack at a Mach Number of 3.12." NASA-TN-3256, July 1954.

10. McCauley, W. D., Saydah, A., and Bueche, J. "The Effect of Controlled Three-Dimensional Roughness on Hypersonic Laminar Boundary Layer Transition." AIAA Preprint No. 66-26, Third Aerospace Sciences Meeting, January 1966.

11. Ericsson, L. E. and Reding, J. P. "Aerodynamic Effects of Bulbous Bases." NASA CR No. 66434, June 1967.

12. Pate, S. R. and Schueler, C. J. "Effects of Radiated Aerodynamic Noise on Model Boundary Layer Transition in Supersonic and Hypersonic Wind Tunnels." AEDC-TR-67-236 (AD666644), March 1968.

13. Brong, E. A. "The Unsteady Flow Field about a Right Circular Cone in Unsteady Flight." FDL-TDR-64-148, January 1967.

14. Rie, H., Linkiewicz, E. A., and Bosworth, F. D. "Hypersonic Dynamic Stability, Part III Unsteady Flow Field Program." FDL-TDR-64-149, Part III, January 1967.

15. Clay, J. T. "Nose Bluntness, Cone Angle, and Mach Number Effects on the Stability Derivatives of Slender Cones." ARL-67-0185, September 1967.

APPENDIXES

I. ILLUSTRATIONS

II. TABLE

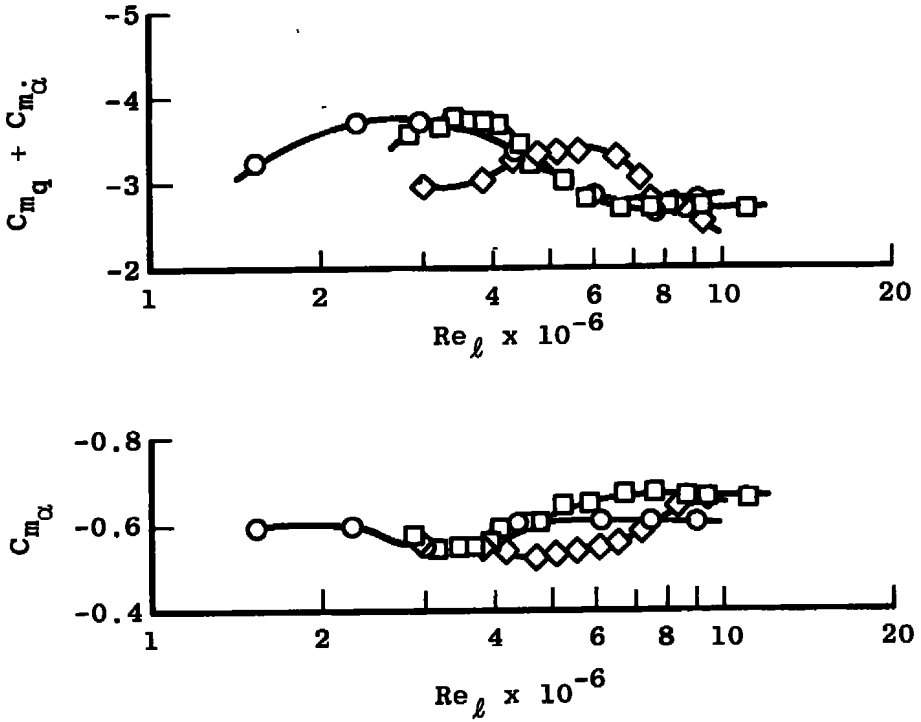

Sym	M_∞	Source	Tunnel	$(\omega d/2V_\infty)$, rad
○	3	Ref. 5	VKF-D	≈ 0.012
□	5	Ref. 6	VKF-E	≈ 0.008
◇	7	Ref. 6	VKF-E	≈ 0.005

$r_n/r_b = 0.0167$
$x_{cg}/\ell = 0.550$
$X_{cg}/L = 0.556$
$\theta = \pm 2$ deg

Fig. 1 Variation of Dynamic and Static Stability Derivatives with Reynolds Number (Reℓ), θ_c = 10 deg

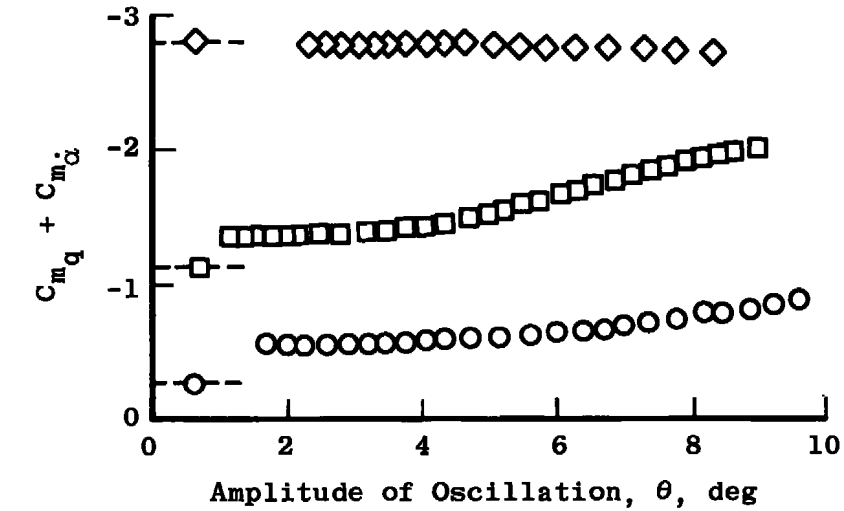

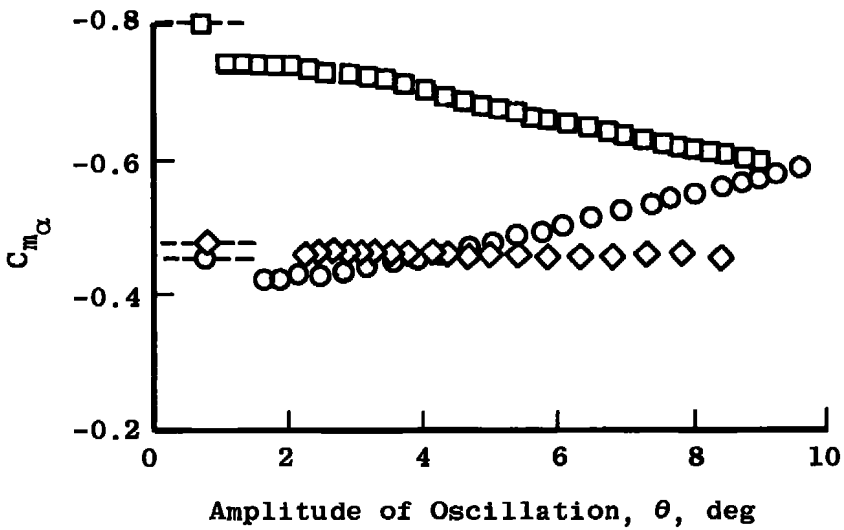

$M_\infty \approx 10$

——— Unsteady Flow Field Theory (Refs. 13 and 14)

Sym	r_n/r_b	x_{cg}/ℓ	X_{cg}/L	$\omega d/2V_\infty$	$Re_\ell \times 10^{-6}$
◇	0.001	0.600	0.600	0.0009	2.42
□	0.151	0.542	0.600	0.0015	3.19
○	0.300	0.465	0.600	0.0012	2.72

Fig. 2 Variation of Dynamic and Static Stability Derivatives with Amplitude of Oscillation

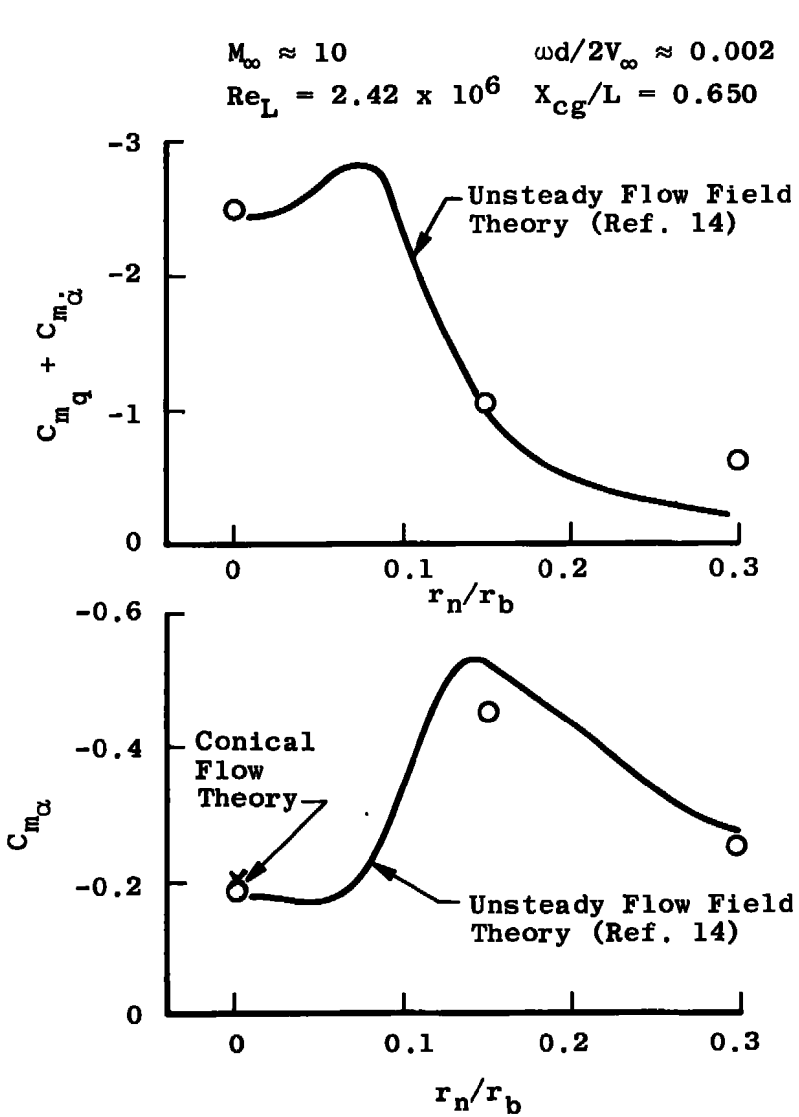

Fig. 3 Variation of $C_{m_q} + C_{m_{\dot\alpha}}$ and C_{m_α} with Nose Bluntness, $\theta_c = 10$ deg, $M_\infty \approx 10$

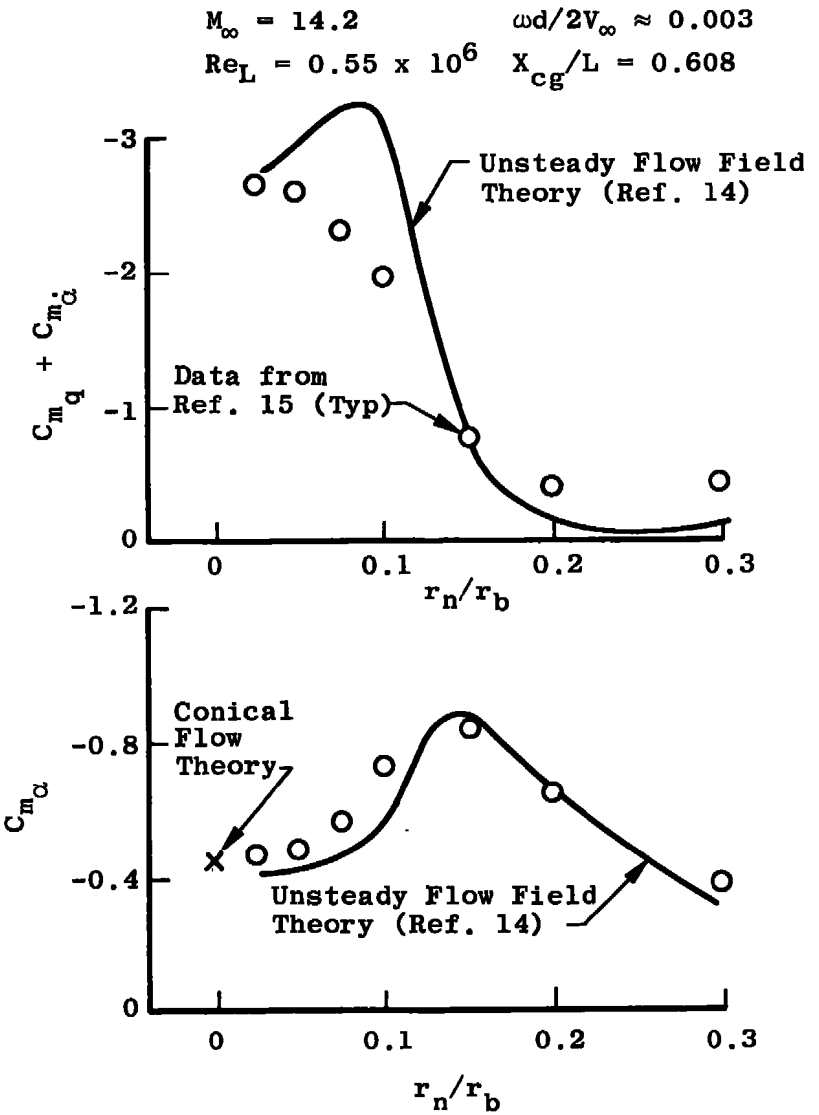

Fig. 4 Variation of $C_{m_q} + C_{m_{\dot\alpha}}$ and C_{m_α} with Nose Bluntness, $\theta_c = 10$ deg, $M_\infty = 14.2$

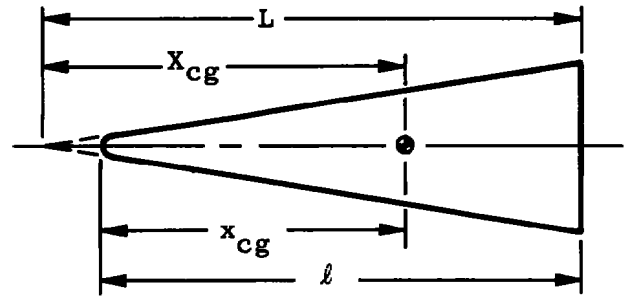

r_n/r_b	x_{cg}/ℓ	X_{cg}/L
0	0.600	0.600
0.04	0.600	0.613
0.08	0.600	0.627

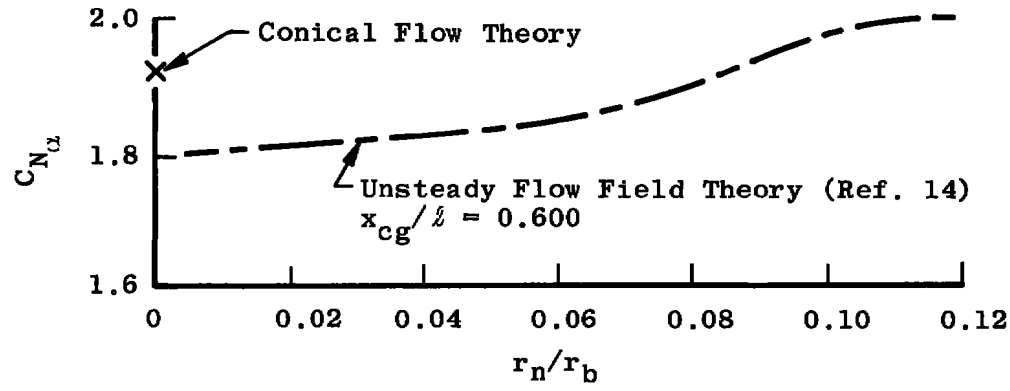

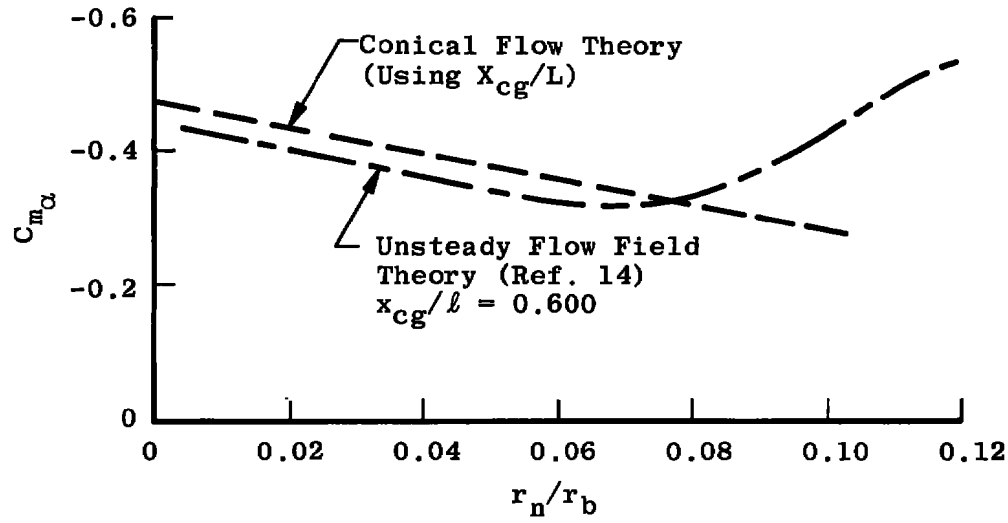

Fig. 5 Theoretical Predictions of C_{N_α} and C_{m_α} as a Function of Nose Bluntness Ratio (r_n/r_b), θ_c = 10 deg, M_∞ = 10

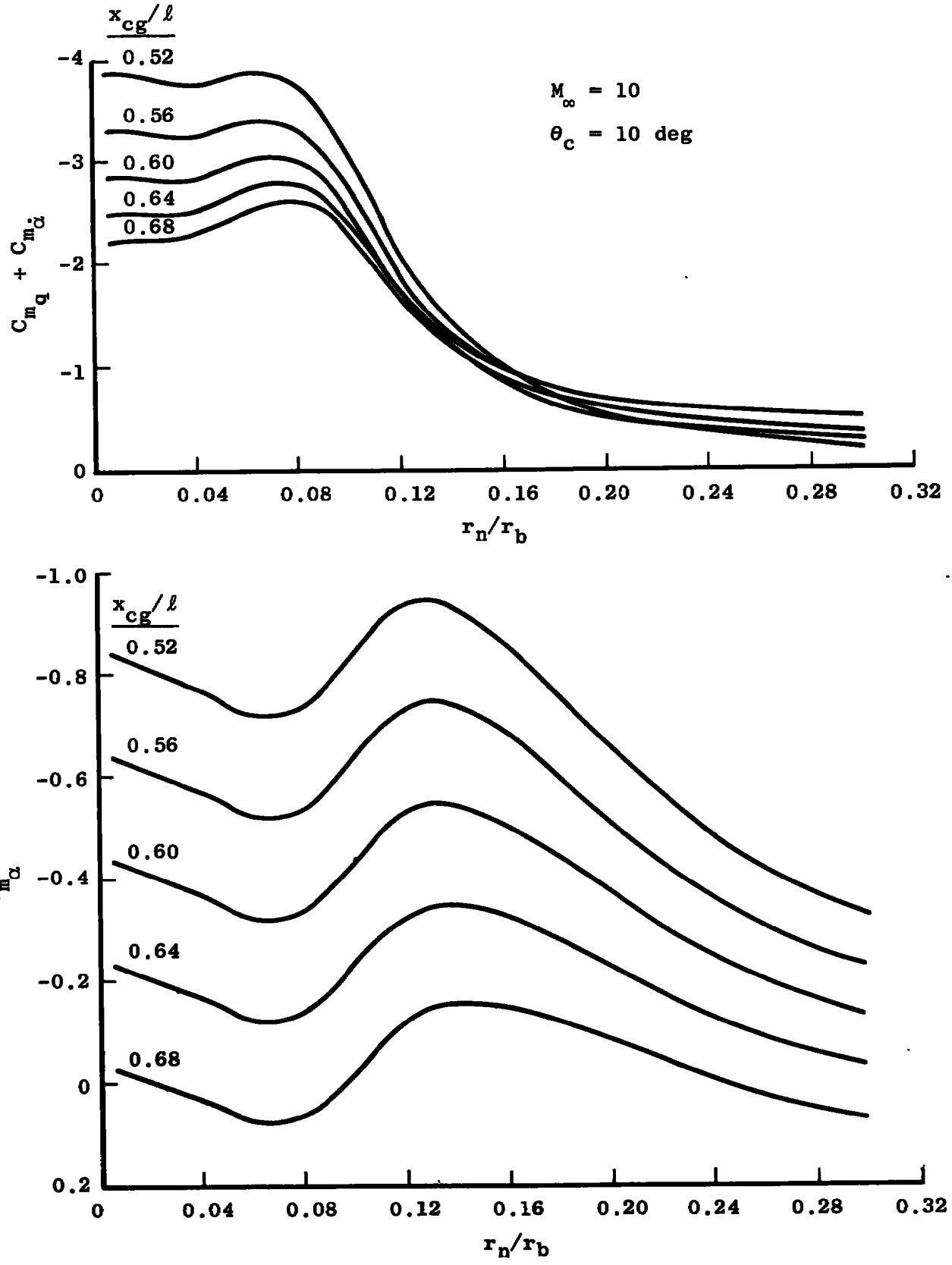

Fig. 6 Unsteady Flow Field Predictions of $C_{m_q} + C_{m_{\dot{\alpha}}}$ and C_{m_α} as a Function of r_n/r_b (from Ref. 14)

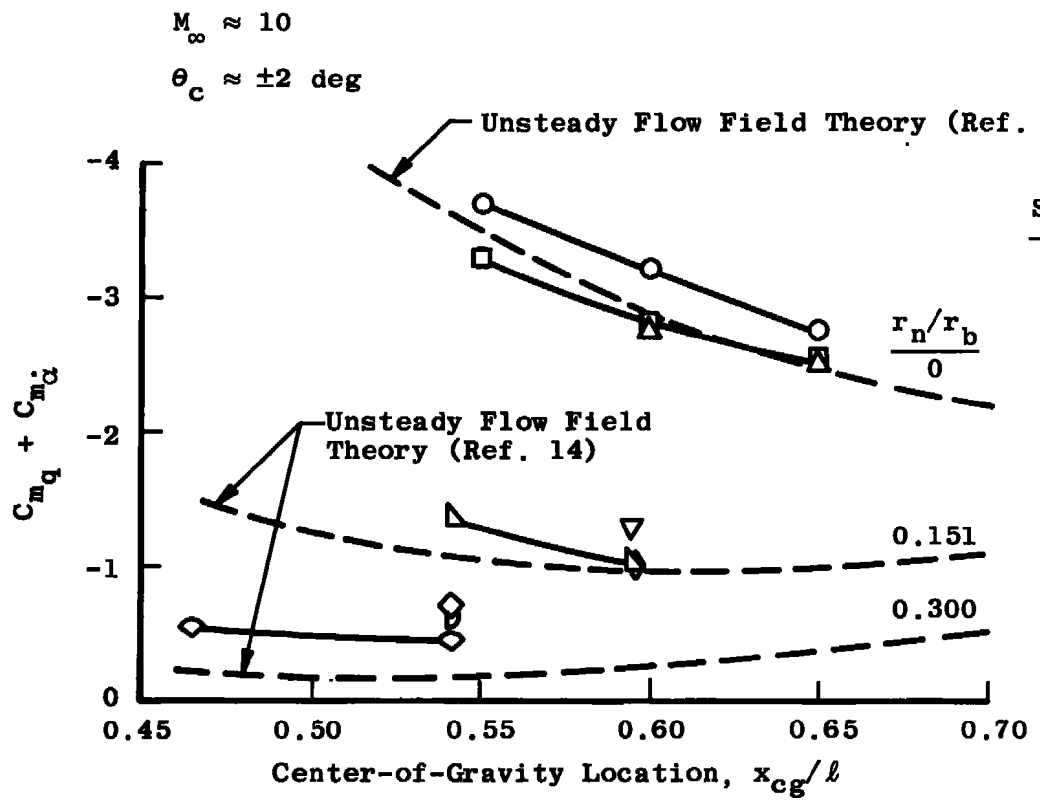

Sym	r_n/r_b	$(\omega d/2V_\infty)10^3$	Type Balance	$Re_\ell \times 10^{-6}$
○	0.001	3.4	Forced	2.42
□	0.001	2.0	Forced	2.42
△	0.001	0.6 to 0.9	Free	2.42
◇	0.151	2.0	Forced	2.10
◺	0.151	1.1 to 1.5	Free	3.19
▽	0.151	3.4	Forced	2.10
◇	0.300	1.0 to 1.2	Free	2.72
◗	0.300	2.0	Forced	1.80
◇	0.300	3.4	Forced	2.24

Fig. 7 Variation of $C_{m_q} + C_{m_{\dot{\alpha}}}$ with Center-of-Gravity Location

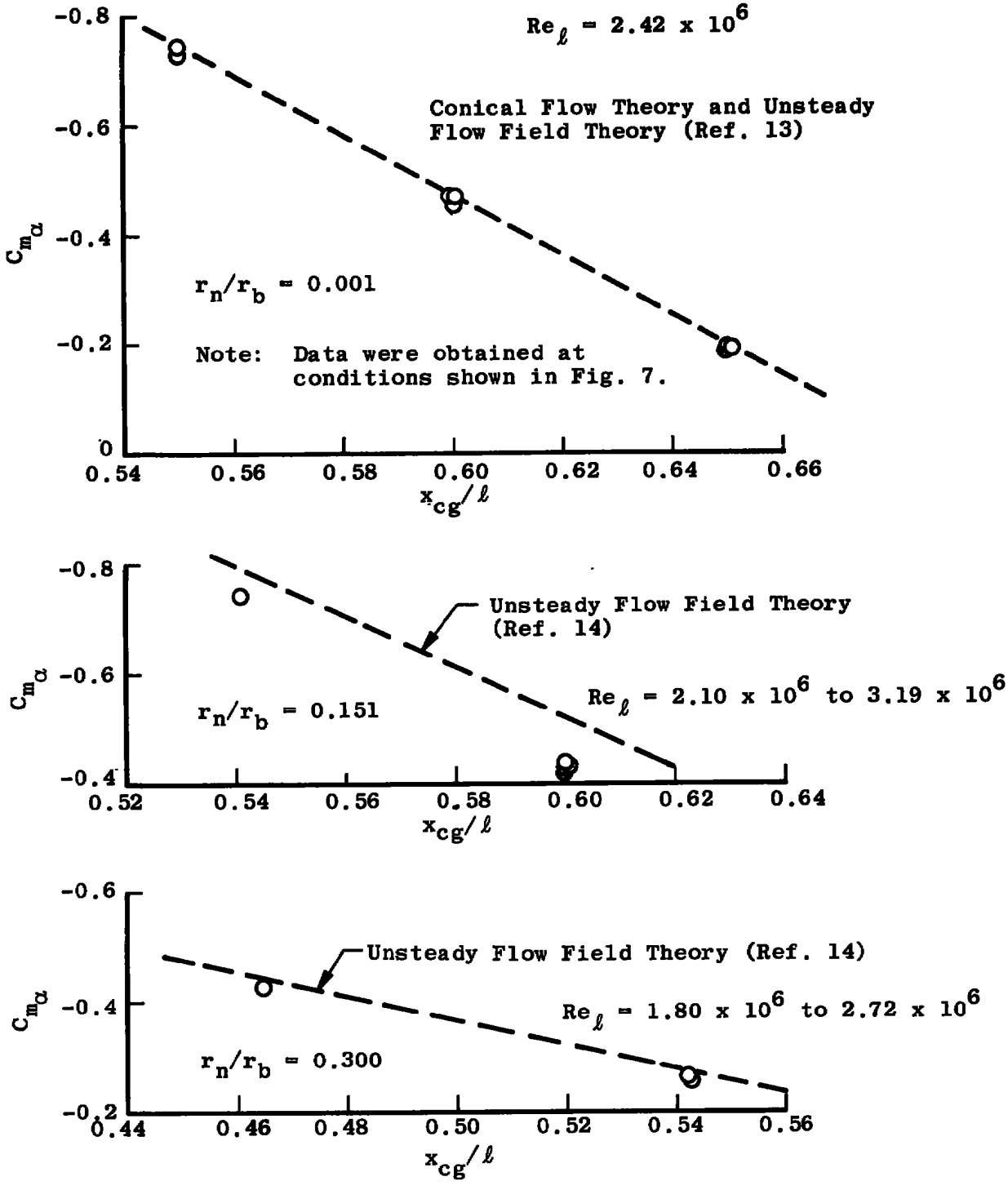

Fig. 8 Variation of C_{m_α} with Center-of-Gravity Location, θ_c = 10 deg, M_∞ = 10, θ = ±2 deg

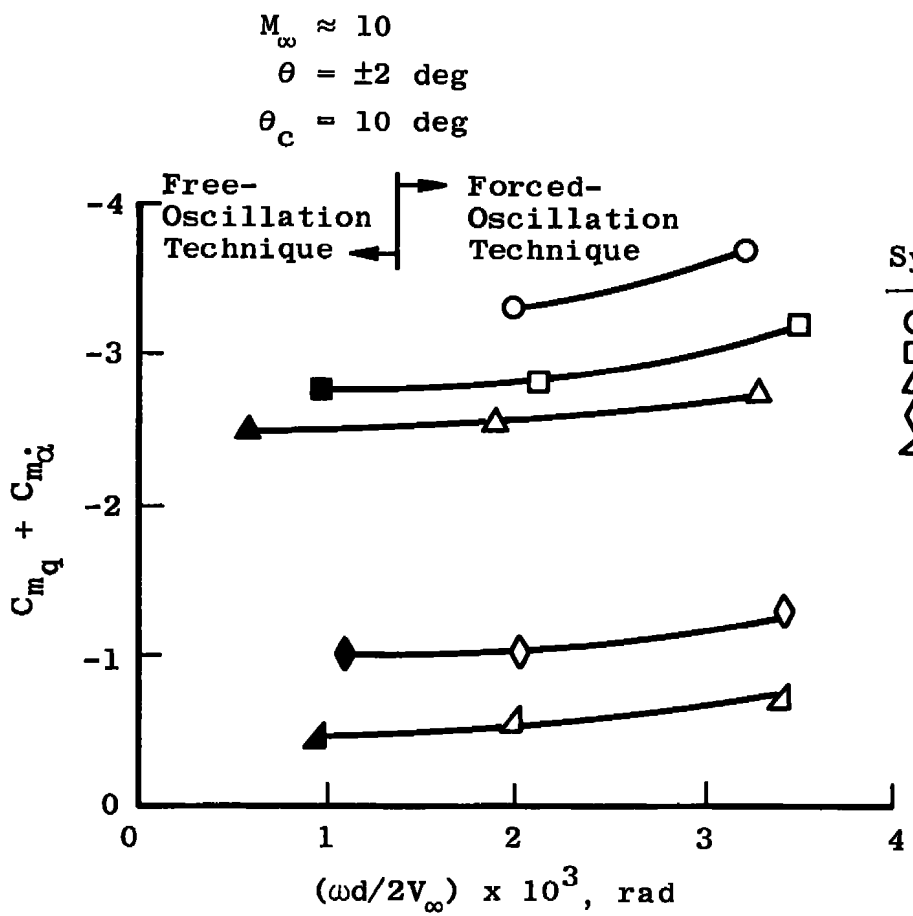

Sym	x_{cg}/ℓ	r_n/r_b	$Re_\ell \times 10^{-6}$
○	0.550	0.001	2.42
□	0.600	0.001	2.42
△	0.650	0.001	2.42
◇	0.595	0.151	2.10 to 3.19
◁	0.542	0.300	1.80 to 2.72

Fig. 9 Variation of $C_{m_q} + C_{m_{\dot{\alpha}}}$ as a Function of $\omega d/2V_\infty$

TABLE I
SUMMARY OF TEST CONDITIONS

Model Conditions

Technique	r_n/r_b	x_{cg}/ℓ	X_{cg}/L	$\approx (Re/\ell) \times 10^{-6}$	$\approx \omega d/2V_\infty \times 10^3$
Forced Oscillation	0.001	0.550, 0.600, 0.650	0.550, 0.600, 0.650	1.02	2.0, 3.4
↓	0.151	0.595	0.650	1.02	2.0, 3.4
↓	0.300	0.542	0.650	1.02, 1.27	2.0, 3.4
Free Oscillation	0.001	0.600, 0.650	0.600, 0.650	1.02	0.6→0.9
↓	0.151	0.542	0.600	1.54	1.5
↓	0.151	0.595	0.650	1.54	1.1
↓	0.300	0.465	0.600	1.54	1.2
↓	0.300	0.542	0.650	1.54	1.0

Tunnel Conditions

$(Re/\ell) \times 10^{-6}$	M_∞	q_∞, psfa	V_∞, ft/sec
1.02	10.12	172	4690
1.27	10.14	215	↓
1.54	10.16	260	

UNCLASSIFIED
Security Classification

DOCUMENT CONTROL DATA - R & D

(Security classification of title, body of abstract and indexing annotation must be entered when the overall report is classified)

1. ORIGINATING ACTIVITY (Corporate author)	2a. REPORT SECURITY CLASSIFICATION
Arnold Engineering Development Center ARO, Inc., Operating Contractor Arnold Air Force Station, Tennessee	UNCLASSIFIED
	2b. GROUP N/A

3 REPORT TITLE

DYNAMIC STABILITY RESULTS FOR SHARP AND BLUNTED 10-DEG CONES AT HYPERSONIC SPEEDS

4 DESCRIPTIVE NOTES (Type of report and inclusive dates)

June 30, 1967 to June 30, 1968 - Final Report

5. AUTHOR(S) (First name, middle initial, last name)

L. K. Ward, Jr. and B. L. Uselton, ARO, Inc.

6 REPORT DATE	7a. TOTAL NO OF PAGES	7b. NO OF REFS
December 1968	27	15

8a. CONTRACT OR GRANT NO.	9a. ORIGINATOR'S REPORT NUMBER(S)
F40600-69-C-0001	
b. G226	AEDC-TR-68-277
c. Program Element 65401F	9b. OTHER REPORT NO(S) (Any other numbers that may be assigned this report)
d	N/A

10 DISTRIBUTION STATEMENT This document is subject to special export controls and each transmittal to foreign governments or foreign nationals may be made only with prior approval of Arnold Engineering Development Center (AETS), Air Force Systems Command, Arnold AF Station, Tennessee 37389.

11 SUPPLEMENTARY NOTES	12 SPONSORING MILITARY ACTIVITY
Available in DDC.	Arnold Engineering Development Center, Air Force Systems Command, Arnold AF Station, Tennessee 37389

13 ABSTRACT

Tests were conducted in Tunnel C of the von Kármán Gas Dynamics Facility to obtain dynamic stability data for sharp and blunted 10-deg half-angle cones. With both a free-oscillation gas bearing pivot balance system and a forced-oscillation cross-flexure pivot balance system, data were obtained at a nominal Mach number of 10 at free-stream Reynolds numbers, based on model length, ranging from 1.80×10^6 to 3.19×10^6. The effects of boundary-layer transition, amplitude of oscillation, nose bluntness, and model center-of-gravity location on the dynamic and static stability derivatives are presented. Comparison of data from the free- and forced-oscillation test techniques and the effect of frequency of oscillation on the damping-in-pitch derivatives are also presented. The derivatives are compared with steady and unsteady flow field theories.

This document is subject to special export controls and each transmittal to foreign governments or foreign nationals may be made only with prior approval of Arnold Engineering Development Center (AETS), Air Force Systems Command, Arnold Air Force Station, Tennessee 37389.

DD FORM 1 NOV 65 1473

UNCLASSIFIED
Security Classification

14 KEY WORDS	LINK A		LINK B		LINK C	
	ROLE	WT	ROLE	WT	ROLE	WT
nose cones						
aerodynamic configurations						
gas bearings						
pivots						
boundary-layer transition						
dynamic stability characteristics						
hypersonic flow						

AFSC
Arnold AFB Tenn